Materials Science and Engineering C 72 (2017) 62–68

Contents lists available at ScienceDirect

Materials Science and Engineering C

journal homepage: www.elsevier.com/locate/msec

Low-temperature thermal reduction of suspended graphene oxide film for electrical sensing of DNA-hybridization

Tun Wang, Hong-chen Guo, Xin-yi Chen *, Miao Lu *

Pen-Tung Sah Institute of Micro-Nano Science & Technology, Xiamen University, 361005, PR China

ARTICLE INFO

Article history:
Received 22 August 2016
Received in revised form 4 October 2016
Accepted 7 November 2016
Available online 09 November 2016

Keywords:
Suspended graphene oxide film
Thermal reduction
DNA detection

ABSTRACT

A reduced graphene oxide (RGO) based capacitive real time bio-sensor was presented. Suspended graphene oxide (GO) film was assembled electrophoretically between the source and drain electrodes of a transistor and then reduced by annealing in hydrogen/nitrogen forming gas to optimize the surface functional groups and conductivity. The resonance frequency of the transmission coefficient (S_{21}) of the transistor was observed to shift with deoxyribonucleic acid (DNA)-hybridization, with a detecting limit of ~5 nM. The advantages of the bio-sensing approach include low-noise frequency output, solution based real time detection and capable of on-chip integration.

1. Introduction

Nanoelectromechanical sensor has attracted much attention in recent years as a label-free, real-time and highly sensitive approach to detect target molecules in solution. These devices measure the deflection of a cantilever or film caused by biomolecules binding to functional groups on the surface of the device, where the deflection of the micromechanical part was detected by optical [1–5], piezoresistive [6–8], piezoelectric [9–11], surface acoustic wave [12,13] or Metal-Oxide-Semiconductor Field Effect Transistor (MOSFET) [14–16], etc. In principle, the sensitivity of the nanoelectromechanical sensor is inversely proportional to the dimensions of the cantilever. Thus, micromechanical parts made up of nanotubes [17,18], nanowires [19,20] or graphene [21,22] are reported in recent. However, it is much more difficult to build a piezoresistive, piezoelectric or MOSFET sensor on nanomaterials than that on silicon. Thus, new deflection detection strategies based on nanomaterials for portable and in-situ applications are desirable.

Well-developed capacitive sensing technology could be used to detect the deflection of a film in the range of a few angstrom straightforwardly [23,24]. The structure of a capacitive deflection sensor is simple, too. For example, a suspended conductive nanomaterial cantilever or film and a solid underneath metal electrode can measure the deflection accurately.

In a previous work, we proposed a nanoelectromechanical biosensor with a suspended single walled carbon nanotubes (SWCNTs) film [25]. However, it is well known that SWCNTs have different sizes, types, chiralities and their orientations are hardly aligned perfectly in the film, which made the repeatability of the biosensor was not satisfied theoretically.

In this paper, we tried to replace the SWCNT film used in ref. 25 with suspended graphene film and investigated its potential applications on bio-sensing. Because Graphene oxide (GO) has good dispersity in water and could be better assembled in the same circumstance than graphene [26,27], the suspended graphene oxide (GO) film was firstly assembled to a transistor-like device with low parasitic capacitance [28]. However, the suspended GO film has low conductivity, which cannot act as a movable electrode of a capacitive sensor. Thus its electrical conductivity needs to be improved by reduction. Unfortunately, most of reported reduction processes of GO are performed at a high temperature or via complicated solution treatments [29–36], in which the device used in this work can be damaged. In that case, we proposed a low temperature and clean reduction process to reduce GO to RGO, while the RGO film could keep freestanding after the process.

As a proof-of-concept of this new biosensor, the hybridization of a single stranded DNA was real-time detected in solution. Comparing with many label-free DNA sensing approaches have been reported in literatures including electrical [37–43], electrochemical [44–48] and optical detection [49–54], the output of this device is based on frequency shift, which has better immunity to environmental interference than voltage or current output. Its driving circuit can also be integrated easily using the commercial CMOS technology with low cost. In addition, the proposed sensor is easy to be integrated to micro fluidic chips by simply coating polydimethylsiloxane (PDMS) channels on its top surface, implying a promising approach for portable, rapid and low cost biosensing.

* Corresponding author.
E-mail addresses: chenxinyi@xmu.edu.cn (X. Chen), lm@xmu.edu.cn (M. Lu).

http://dx.doi.org/10.1016/j.msec.2016.11.026
0928-4931/

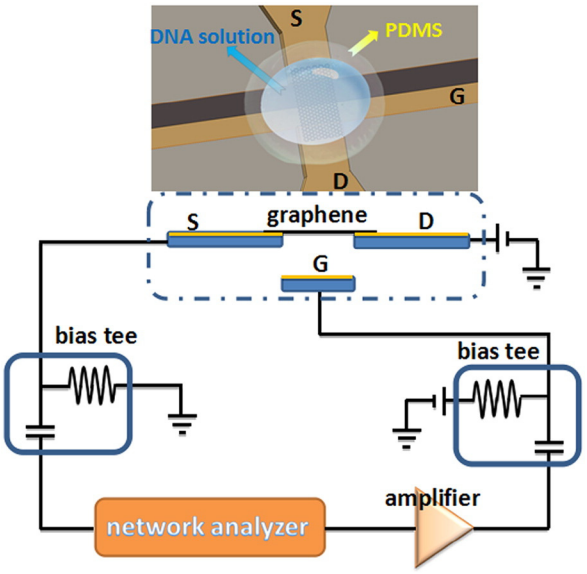

Fig. 1. Schematic of characterization of the proposed DNA sensor based on suspended RGO film.

2. Experimental

2.1. Materials

The well-dispersed solution of graphene oxide was synthesized via modified Hummers' method [55,56] and the concentration was about 20 μg/mL.

Single stranded probe and complementary DNAs were purchased from Invitrogen Biotechnology Co. Ltd. Their sequences and modifications are as follows: probe DNA: 5′-NH_2-$(CH_2)_6$-CGC CGA TTG GAC AAA ACT TAA A-3′; complementary DNA: 5′-FAM-T TTA AGT TTT GTC CAA TCG GCG-3′.

The single stranded probe DNA was dissolved into the immobilization buffer (1.5 mM NaCl + 0.1 mM $NaHCO_3$) to get probe DNA solution. Another single stranded complementary DNA was dissolved into the hybridization buffer (0.15 mM NaCl + 0.015 mM $C_6H_5Na_3O_7 \cdot 2H_2O$ + 2 mg/L SDS ($C_{12}H_{25}SO_4Na$)) to get D'FAM DNA solution.

2.2. Device fabrication

A bi-layer gate electrode (Cr/Au) was formed by sputtering and lift-off on a glass wafer. Next, a 2 μm thick photo resist layer (SU8-2002, MicroChem Corp. USA) was patterned by backside exposing using the gate electrode as photo mask. Another photo resist AZ4620 was then

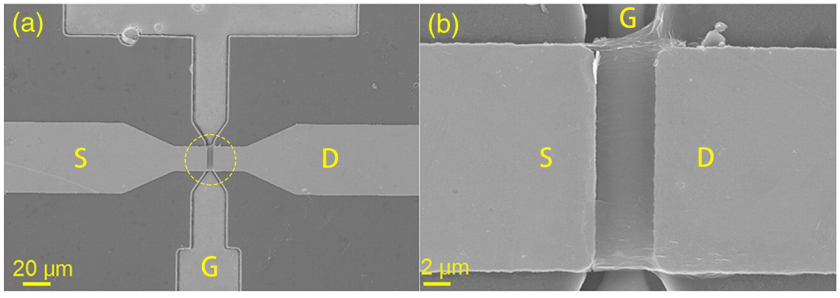

Fig. 2. SEM images of (a) as-assembled GO device; (b) annealed RGO device.

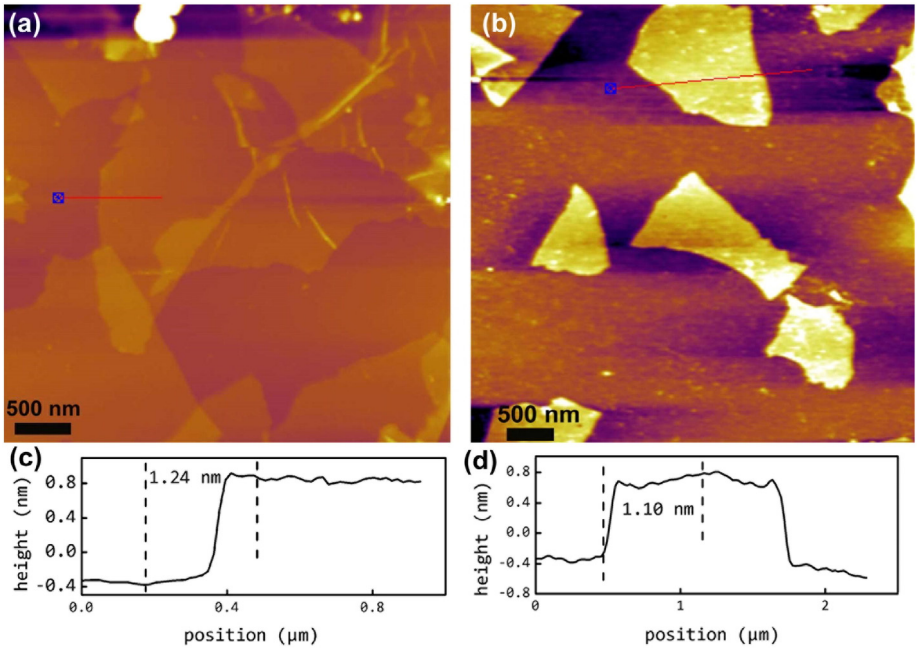

Fig. 3. AFM images of (a) GO and (b) RGO. The thicknesses of (c) GO and (d) RGO nanosheets were 1.24 nm and 1.10 nm, respectively.

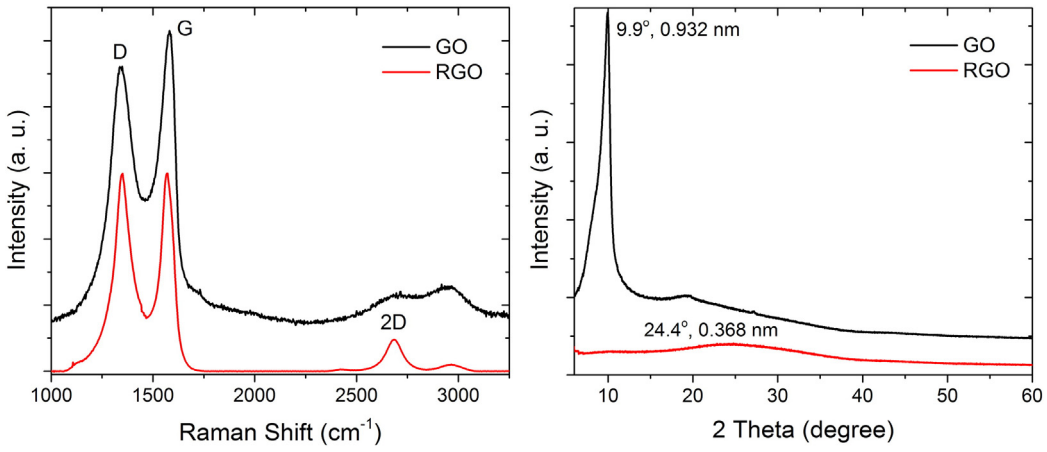

Fig. 4. (a) Raman spectroscopy (a) and (b) XRD patterns of GO and RGO.

spin-coated and polished subsequently to expose the SU8 surface and fill in the gaps between SU-8 patterns. The source and drain electrodes with bilayer of chromium (20 nm) and gold (200 nm) was formed on the surface of SU8 by another sputtering, photolithography and wet etching. Finally, the glass wafer was diced into chips, rinsed by acetone, isopropyl alcohol (IPA) and deionized (DI) water and blown dry by nitrogen.

2.3. Assembly of suspended graphene oxide film

Suspended GO film was assembled between source and drain electrodes of the self-aligned device by dielectrophoresis: 10 μL GO solution (~20 μg/mL) was dropped on the device by a square wave ac signal (200 kHz, 8 Vpp) applying between two electrodes for 4 min. The device was rinsed by DI water and blown dry by nitrogen.

2.4. Hydrogen reduction and characterization of GO film and devices

The devices were annealed in a tube furnace (OTF-1200X-S-DVD, MTI KJ GROUP, China) in 5% hydrogen/95% nitrogen forming gas for 30 min at 180 °C, 190 °C, 200 °C, 210 °C, 240 °C, and 250 °C respectively. After that, the furnace was cooled down to 100 °C in 30 min then to room temperature naturally. A 2-hour annealing at 200 °C was also applied to further increase the conductivity. Scanning electron microscopy (SEM, Carl Zeiss, Germany) and atomic force microscopy (AFM, OXFORD Cypher S, UK) were employed to characterize the morphology. Raman spectroscopy (IDSpec ARCTIC) and X-Ray diffraction (XRD, Shimadzu, Japan) were employed to analyze the structure and surface chemistry of GO and RGO.

The output and transition characteristic curves of the devices before and after thermal reduction were measured by a probe station connecting to a semiconductor parameter analyzer (Keithley 4200, USA). The resistance of the RGO film with different thermal reduction conditions were measured at $V_{ds} = 1.0$ V, $V_{gs} = 0$ V.

2.5. Electrical detection of DNA immobilization and hybridization

The circuit shown in Fig. 1 was employed to characterize the DNA sensor based on suspended RGO film. A sweeping high frequency signal from a vector network analyzer (ZNB 8, R&S) was applied between the gate and the grounded source (acting as the input port) through bias T respectively. The signal fed back into the network analyzer after passing through the drain. A low-noise preamplifier (Agilent 8447D) provided 25 dB gain and DC bias about 1.0 V was applied to the drain.

The detection of DNA immobilization was performed by dropping 10 μL probe DNA solution with a certain concentration (5 μM, 5 nM, 50 nM, 500 nM) onto the top surface of as-prepared devices, which was followed by 30 μL PDMS primer dropping on the same location to encapsulate the DNA solution to prevent evaporation. The transmission coefficient S_{21} was recorded in each 5 min to observe the real-time DNA immobilization for an hour.

Electrical detection of DNA hybridization was performed as follows: the devices were immersed in the as-mentioned probe DNA solution (5 μM in 2 mL immobilization buffer) overnight to ensure a full coverage of probe DNA on the surface of RGO, then rinsed with immobilization buffer. After that, the complementary DNA solution (10 μL) with the concentration of 5, 50, 500 nM and 5 μM were dropped on the top surface of the device, respectively, followed by 30 μL PDMS primer to prevent solution evaporation. The transmission coefficient S_{21} was recorded every 5 min for an hour to reveal the real-time hybridization of complementary DNA with probe DNA.

3. Results and discussion

3.1. Surface characterizations

Fig. 2 showed the SEM images of the as-assembled GO device and the annealed RGO device, respectively. The GO film was assembled between the source and drain as indicated in the central area of Fig. 2(a). Using the fabrication methods mentioned in 2.2 paragraph, the gap between the two gold electrodes (source and drain) was found to close to 4 μm for each chip that we fabricated. Under the assembly condition

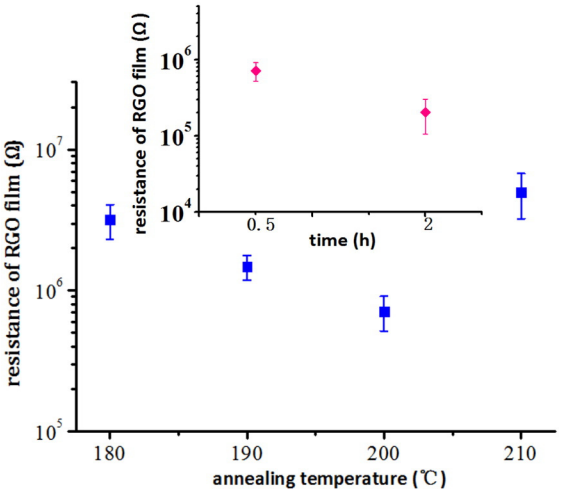

Fig. 5. Resistance of RGO film annealed for 30 min at different temperatures. The inset shows the resistance of RGO film after thermal reduction at 200 °C but for 30 min and 2 h, respectively.

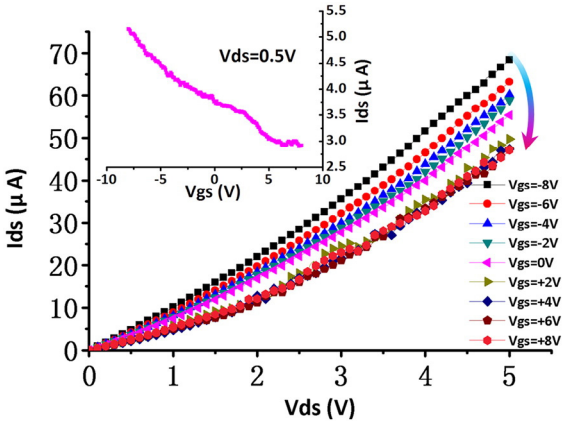

Fig. 6. The output and transition characteristic curve of the device after thermal reduction at 200 °C for 2 h at hydrogen atmosphere.

listed in 2.3 paragraph, the suspended graphene oxide film was found to be assembled almost every time by dielectrophoresis in this experiment.

It was also found that the morphology of GO film did not change obviously after annealing. However, the RGO film was found broken at 240 °C, 250 °C (not shown) and kept uniform below 210 °C, which was theoretically expected because of the thermal mismatch between RGO film and the device. AFM images of GO and RGO were shown in Fig. 3, from which the thickness of the GO and RGO nanosheet could also be measured. Fig. 3(c) indicated that the thickness of GO nanosheet was about 1.24 nm. Fig. 3(d) showed that the thickness of the annealed RGO nanosheet was about 1.10 nm, which was comparable to that of the as-prepared GO nanosheet.

The structure and surface properties of GO and RGO were characterized by Raman spectroscopy (laser wavelength, 532 nm) and XRD, as shown in Fig. 4. In the Raman spectra, the peak at ~1350 cm^{-1} corresponding to disorder and crystal size of graphite structure (D peak), as well as the peak at ~1580 cm^{-1} corresponding to the C-sp^2 honeycomb structure (G peak), could be identified in both GO and RGO, while the I_D/I_G ratio increased from GO to RGO, which might be caused by the loss of carbon and transition of oxygenated functional groups during the annealing [57,58]. Meanwhile, the G peak shifted from ~1581 cm^{-1} to 1571 cm^{-1}, and the characteristic peak of graphene at 2685 cm^{-1} (2D peak) was observed in RGO [57–59], indicating a successful reduction from GO to RGO via the hydrogen annealing. On the other hand, the XRD pattern also confirmed the reduction i.e. GO exhibited a sharp 2θ peak at 9.9° corresponding to the interlayer distance of GO [60], while that of RGO showed a weak broad peak at ~24.4° attributed to distance of graphite sheets along [001]. Particularly, it should be noticed that the 2D peak of RGO was a sharp single peak around 2685 cm^{-1}, which indicated that the RGO film assembled to the device was highly possible to be a monolayer RGO [58,59].

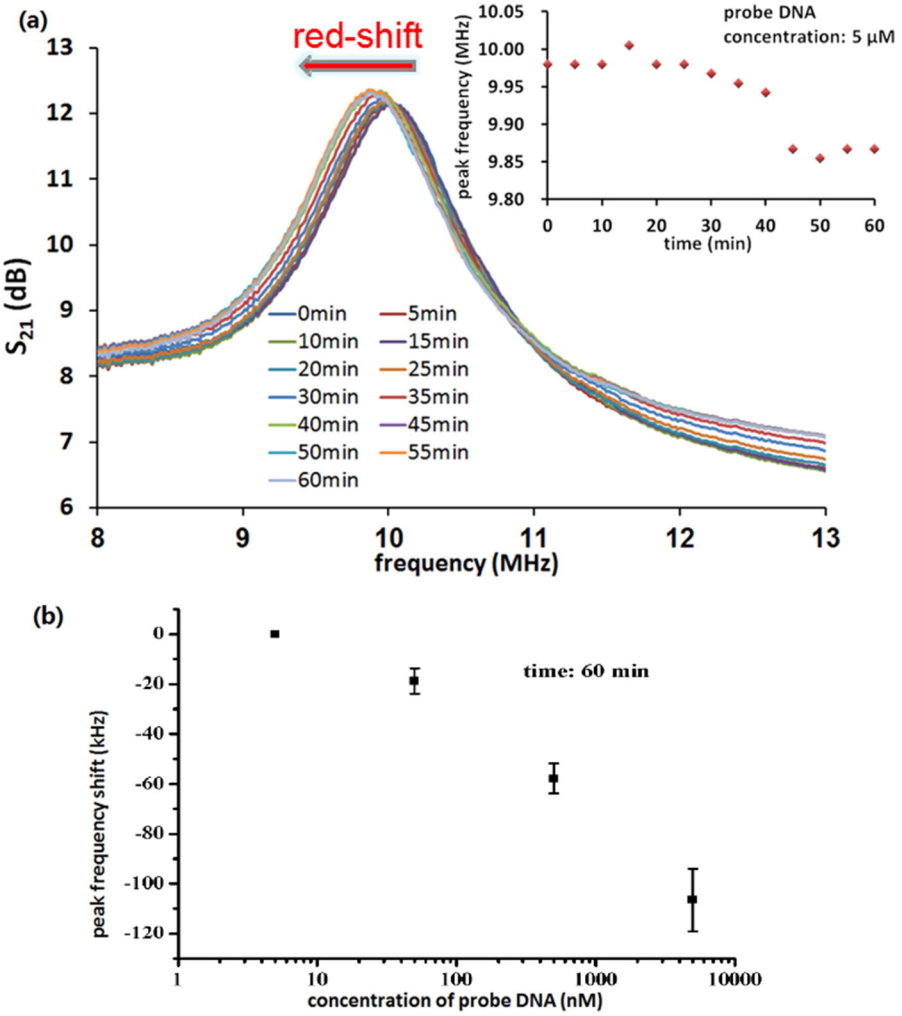

Fig. 7. (a) The red-shift of resonance frequency after the probe DNA was dropped on the suspending RGO film of the device. (b) The shift of resonance frequency versus the concentration of probe DNA. Each data was collected 1 h after the probe DNA was dropped on the suspending RGO film of the device. (For interpretation of the references to colour in this figure legend, the reader is referred to the web version of this article.)

3.2. Electrical characterization of the suspended RGO film

Fig. 5 showed the resistance of RGO films i.e. GO films after 30 min annealing at 180 °C, 190 °C, 200 °C, and 210 °C, respectively. It should be noticed that the resistance of GO film exceeds 10^{12} Ω. The minimized average resistance of the suspended RGO film occurred after annealing at 200 °C, which was about 770 kΩ. The inset in Fig. 5 showed the resistance of RGO film after thermal reduction at 200 °C for 30 min and 2 h, respectively. The resistance decreased to 150 kΩ with extending the annealing time to 2 h.

The resistance of the suspended GO film on the device was over 10^{12} Ω, which was in consistence with the reported square resistance of GO (~10^{12} Ω/sq) in previous literature [61,62]. The electrical conductivity of RGO film after thermal annealing had a typical mean value of 20 S/cm when the annealing temperature was 200 °C. This is less than the reported 727 S/cm after 1100 °C annealing [63] because the annealing temperature in our experiment was much lower. The resistance of the RGO film increased abnormally when the annealing temperature exceeded 200 °C as shown in Fig. 5. The main reason was that small cracks were found on suspended RGO film due to the thermal mismatch between RGO and the substrate at higher annealing temperature.

The output and transition curves of the RGO film annealed at 200 °C were measured to determine the electrical properties as shown in Fig. 6. In the output characteristic curve, the V_{gs} changed from −8 V to 8 V, while the V_{ds} sweeping from zero to 5 V. In the transition curve, the V_{ds} was set to 0.5 V, and Vgs was swept from −8 V to 8 V. As a result, the resistance of the suspending RGO film increased by approximately 75%. The device exhibited a p-type semiconductor behavior due to the oxygenated surface functional groups, which is consistent with the previous result [64].

3.3. Detection of DNA

The resonant frequency of RGO devices immobilized with probe DNA was firstly measured to obtain the reference frequency for the following detection. Fig. 7(a) showed the time-dependent change of resonance frequency after the probe DNA (5 μM, 10 μL) was dropped on the suspending RGO film. The frequency remained the same value at approximately 9.98 MHz in the first 20 min, then decreased to 9.86 MHz slowly in the following 30 min. Fig. 7(b) showed the dependence of resonance frequency and concentrations of probe DNA solution. It could be concluded that a higher red-shift occurred with a higher concentration

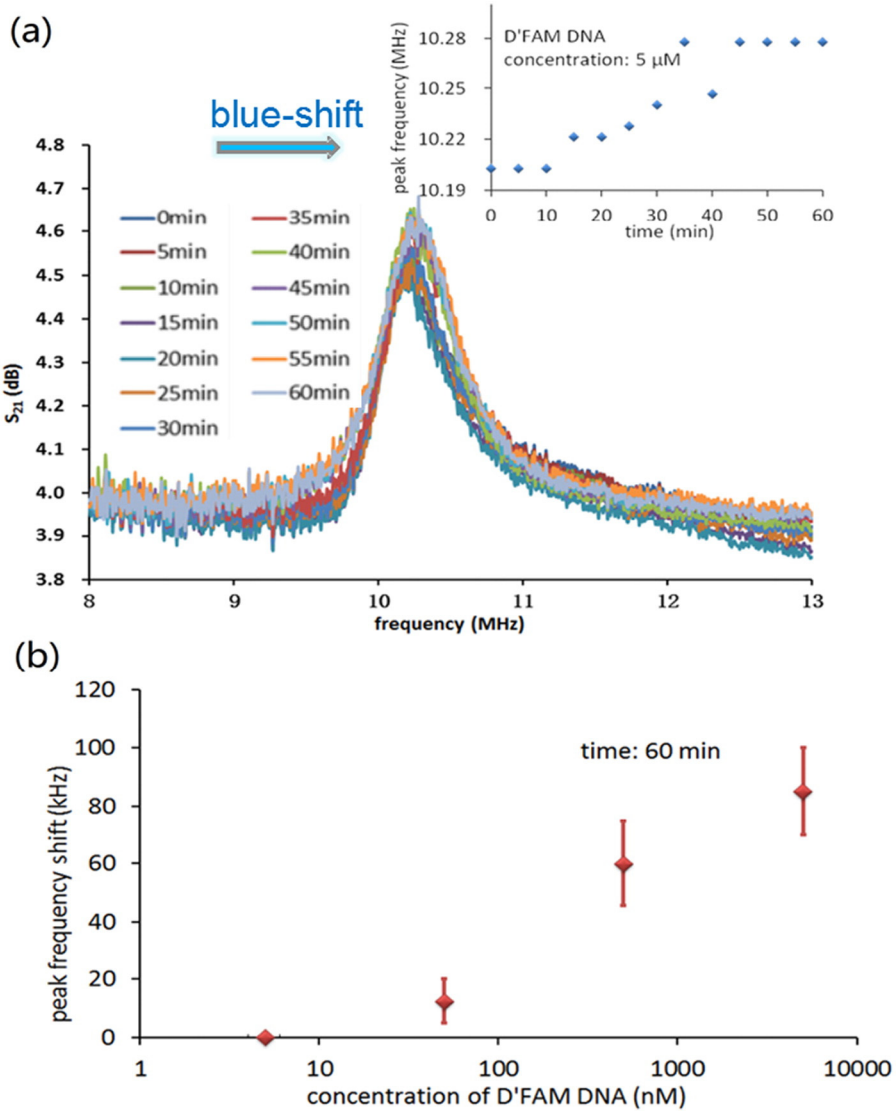

Fig. 8. (a) The blue-shift of resonance frequency versus time after 10 μL, 5 μM complementary DNA was dropped on the suspending RGO film of the device. (b) The shift of resonance frequency versus the concentration of complementary DNA. Each data was collected one hour after the probe DNA was dropped on the suspending RGO film of the device. (For interpretation of the references to colour in this figure legend, the reader is referred to the web version of this article.)

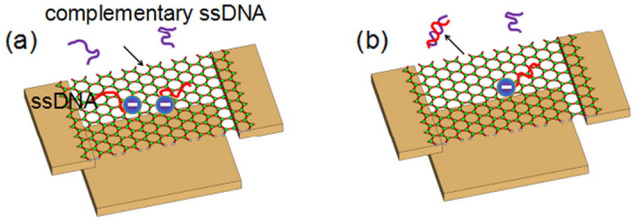

Fig. 9. Mechanism of the DNA biosensing on RGO film: (a) ssDNA was immobilized onto the surface of RGO film and additional charges generated, and (b) DNA hybridization happened and additional charges were bought out of the RGO film.

of probe DNA. The shift of resonance frequency was almost zero at the concentration of 5 nM, which could reach 120 kHz while the concentration of probe DNA was 5 μM.

Secondly, the blue-shift of resonance frequency attributed to the drop of 10 μL, 5 μM complementary DNA solution on the device, as shown in Fig. 8. The resonance frequency was constant in the first 10 min and then increased from 10.20 MHz to 10.28 MHz. After 50 min, the resonance frequency remained the same value because of the saturation of the hybridization. In the hybridization process, the probe DNA was desorbed from the RGO film, which reinstated the surface charges of the RGO film and increased the resonance frequency.

Fig. 8(b) indicated that the resonance frequency increased with the increase of the concentration of complementary DNA i.e. a positive correlation. The average blue-shift could reach 90 kHz after 10 μL, 5 μM complementary DNA was dropped on the device for 1 h. The detecting limit of the device would be as low as 5 nM.

The interaction between DNA and RGO film was illustrated in Fig. 9. Previous studies showed that the interaction between graphene and single-stranded DNA produced stable negative charges because the phosphate groups on the DNA backbones were deprotonated (Fig. 9a) [65,66]. When the complementary ssDNA was introduced onto the same RGO film and bound probe ssDNA, the double stranded DNA (dsDNA) could not stably bind onto the RGO film because of the existence of efficient shielding of nucleobases [67]. As illustrated in Fig. 9b, the negative charges on the suspended RGO film will decrease with the DNA hybridization resulting in variation of electrostatic force between the suspended RGO film and the underneath gate. This varied electrostatic force will further change their gapping distance caused by the deflected RGO film. As a result, the gate capacitance would change. The resonance peak of transmission coefficient S_{21} depends on the gate capacitance and channel conductance in this configuration, so the DNA hybridization on RGO film could generate a frequency shift of S_{21}.

4. Conclusion

A detection method of DNA immobilization and hybridization utilizing suspended RGO film based transistor was presented. The transmission coefficient S_{21} of the device was measured and its resonance frequency was observed to decrease for DNA immobilization and to increase for hybridization. A capacitive sensing mechanism was proposed that the variation of surface charge in the process of DNA immobilization and hybridization deflected the suspended RGO film and further varied the gate capacitance, leading to the shift of the resonance frequency.

In general, this study demonstrates a practical method of combining the use of suspended RGO film and capacitive electrical detection in sensitive and fast detection of DNA hybridization.

Acknowledgments

This work was supported by the NSFC under project No. 61071010, the Fundamental Research Funds for the Central Universities (No. 20720150084), the Natural Science Foundation of Fujian Province of China (No. 2015J05130), and Young Teachers' Education and Research Project of Department of Education of Fujian Province (No. JA14007).

References

[1] J.L. Arlett, E.B. Myers, M.L. Roukes, Comparative advantages of mechanical biosensors, Nat. Nanotechnol. 6 (2011) 203–215.
[2] H. Hou, X.J. Bai, C.Y. Xing, B.P. Lu, J.H. Hao, X. Ke, N.Y. Gu, B.L. Zhang, J.L. Tang, Label-free detection of single-stranded DNA binding protein based on a cantilever array, Talanta 109 (2013) 173–176.
[3] F. Huber, H. Lang, N. Backmann, D. Rimoldi, C. Gerber, Direct detection of a BRAF mutation in total RNA from melanoma cells using cantilever arrays, Nat. Nanotechnol. 8 (2013) 125–129.
[4] K.L. Pirozzi, C.J. Long, C.W. McAleer, A.S.T. Smith, J.J. Hickman, Correlation of embryonic skeletal muscle myotube physical characteristics with contractile force generation on an atomic force microscope-based bio-microelectromechanical systems device, Appl. Phys. Lett. 103 (2013).
[5] B. Wang, F.L. Huang, T. Nguyen, Y. Xu, Q. Lin, Microcantilever-based label-free characterization of temperature-dependent biomolecular affinity binding, Sensor Actuators B Chem. 176 (2013) 653–659.
[6] B.N. Johnson, R. Mutharasan, Reduction of nonspecific protein adsorption on cantilever biosensors caused by transverse resonant mode vibration, Analyst 139 (2014) 1112–1120.
[7] M. Joshi, P.S. Gandhi, R. Lal, V.R. Rao, S. Mukherji, Modeling, simulation, and design guidelines for piezoresistive affinity cantilevers, J. Microelectromech. S 20 (2011) 774–784.
[8] T.G. Xu, H.T. Yu, P.C. Xu, W.J. Xu, W.Q. Chen, C.Z. Chen, X.X. Li, Real-time enzyme-digesting identification of double-strand DNA in a resonance-cantilever embedded micro-chamber, Lab Chip 14 (2014) 1206–1214.
[9] B.N. Johnson, R. Mutharasan, Sample preparation-free, real-time detection of microRNA in human serum using piezoelectric cantilever biosensors at Attomole level, Anal. Chem. 84 (2012) 10426–10436.
[10] D. Lee, K.S. Hwang, S. Kim, T. Thundat, Rapid discrimination of DNA strands using an opto-calorimetric microcantilever sensor, Lab Chip 14 (2014) 4659–4664.
[11] K. Rijal, R. Mutharasan, A method for DNA-based detection of *E. coli* O157:H7 in a proteinous background using piezoelectric-excited cantilever sensors, Analyst 138 (2013) 2943–2950.
[12] G. De Simoni, G. Signore, M. Agostini, F. Beltram, V. Piazza, A surface-acoustic-wave-based cantilever bio-sensor, Biosens. Bioelectron. 68 (2015) 570–576.
[13] K. Lange, B.E. Rapp, M. Rapp, Surface acoustic wave biosensors: a review, Anal. Bioanal. Chem. 391 (2008) 1509–1519.
[14] Y.J. Huang, C.W. Huang, T.H. Lin, C.T. Lin, L.G. Chen, P.Y. Hsiao, B.R. Wu, H.T. Hsueh, B.J. Kuo, H.H. Tsai, H.H. Liao, Y.Z. Juang, C.K. Wang, S.S. Lu, A CMOS cantilever-based label-free DNA SoC with improved sensitivity for hepatitis B virus detection, IEEE. T. Biomed. Circ. S. 7 (2013) 820–831.
[15] M.S. Islam, A.Z. Kouzani, Design of a high sensitive double-gate field-effect transistor biosensor for DNA detection, 2011 Annual International Conference Of the Ieee Engineering In Medicine And Biology Society (Embc) 2011, pp. 4788–4791.
[16] S. Rabbani, P. Brishbhan, Cantilever embedded Mosfet for bio-sensing, 2011 24th Canadian Conference on Electrical And Computer Engineering (Ccece) 2011, pp. 489–492.
[17] Y.W. Lan, L.N. Nguyen, S.J. Lai, M.C. Lin, C.H. Kuan, C.D. Chen, Identification of embedded charge defects in suspended silicon nanowires using a carbon-nanotube cantilever gate, Appl. Phys. Lett. 99 (2011).
[18] N. Matsunaga, T. Arie, S. Akita, A carbon nanotube field-effect transistor with a cantilevered carbon nanotube gate, Appl. Phys. Express 5 (2012).
[19] C. Canetta, S. Guo, A. Narayanaswamy, Measuring thermal conductivity of polystyrene nanowires using the dual-cantilever technique, Rev. Sci. Instrum. 85 (2014).
[20] S.S. Zhang, L. Lou, C. Lee, Piezoresistive silicon nanowire based nanoelectromechanical system cantilever air flow sensor, Appl. Phys. Lett. 100 (2012).
[21] A. Reserbat-Plantey, L. Marty, O. Arcizet, N. Bendiab, V. Bouchiat, A local optical probe for measuring motion and stress in a nanoelectromechanical system, Nat. Nanotechnol. 7 (2012) 151–155.
[22] J. You, K. Jang, S. Lee, D. Bang, S. Haam, C.H. Choi, J. Park, S. Na, Label-free detection of zinc oxide nanowire using a graphene wrapping method, Biosens. Bioelectron. 68 (2015) 481–486.
[23] S.I. Moore, S.O.R. Moheimani, Displacement measurement with a self-sensing MEMS electrostatic drive, J. Microelectromech. Syst. 23 (2014) 511–513.
[24] S. Nihtianov, Measuring in the subnanometer range capacitive and Eddy current nanodisplacement sensors, IEEE. Ind. Electron. M. 8 (2014) 6–15.
[25] T. Wang, Z. Zheng, X. Feng, H. Chen, M. Lu, Electrical sensing of DNA-hybridization using two-port network based on suspended carbon nanotube membrane, Biomed. Microdevices 17 (2015) 103–109.
[26] Y. Si, E.T. Samulski, Synthesis of water soluble graphene, Nano Lett. 8 (2008) 1679–1682.
[27] T. Wei, G.L. Luo, Z.J. Fan, C. Zheng, J. Yan, C.Z. Yao, W.F. Li, C. Zhang, Preparation of graphene nanosheet/polymer composites using in situ reduction-extractive dispersion, Carbon 47 (2009) 2296–2299.
[28] T. Wang, B. Liu, S. Jiang, H. Rong, M. Lu, A local bottom-gate structure with low parasitic capacitance for dielectrophoresis assembly and electrical characterization of suspended nanomaterials, J. Micromech. Microeng. 24 (2014) 055025.
[29] W.F. Chen, L.F. Yan, In situ self-assembly of mild chemical reduction graphene for three-dimensional architectures, Nanoscale 3 (2011) 3132–3137.
[30] R. Larciprete, S. Fabris, T. Sun, P. Lacovig, A. Baraldi, S. Lizzit, Dual path mechanism in the thermal reduction of graphene oxide, J. Am. Chem. Soc. 133 (2011) 17315–17321.

[31] S. Park, J. An, J.R. Potts, A. Velamakanni, S. Murali, R.S. Ruoff, Hydrazine-reduction of graphite- and graphene oxide, Carbon 49 (2011) 3019–3023.
[32] K.X. Sheng, Y.X. Xu, C. Li, G.Q. Shi, High-performance self-assembled graphene hydrogels prepared by chemical reduction of graphene oxide, New Carbon Mater. 26 (2011) 9–15.
[33] P. Song, X.Y. Zhang, M.X. Sun, X.L. Cui, Y.H. Lin, Synthesis of graphene nanosheets via oxalic acid-induced chemical reduction of exfoliated graphite oxide, RSC Adv. 2 (2012) 1168–1173.
[34] T. Sun, S. Fabris, S. Baroni, Surface precursors and reaction mechanisms for the thermal reduction of graphene basal surfaces oxidized by atomic oxygen, J. Phys. Chem. C 115 (2011) 4730–4737.
[35] Z.L. Wang, D. Xu, Y. Huang, Z. Wu, L.M. Wang, X.B. Zhang, Facile, mild and fast thermal-decomposition reduction of graphene oxide in air and its application in high-performance lithium batteries, Chem. Commun. 48 (2012) 976–978.
[36] Z.S. Wu, S.B. Yang, Y. Sun, K. Parvez, X.L. Feng, K. Mullen, 3D nitrogen-doped graphene aerogel-supported Fe_3O_4 nanoparticles as efficient eletrocatalysts for the oxygen reduction reaction, J. Am. Chem. Soc. 134 (2012) 9082–9085.
[37] M.H. Abouzar, A. Poghossian, A.G. Cherstvy, A.M. Pedraza, S. Ingebrandt, M.J. Schoning, Label-free electrical detection of DNA by means of field-effect nanoplate capacitors: experiments and modeling, Phys. Status Solidi A 209 (2012) 925–934.
[38] T.Y. Chen, T.K.L. Phan, C.L. Hsu, Y.H. Lee, J.T.W. Wang, K.H. Wei, C.T. Lin, L.J. Li, Label-free detection of DNA hybridization using transistors based on CVD grown graphene, Biosens. Bioelectron. 41 (2013) 103–109.
[39] J.-M. Choi, S.-U. Hwang, C.-H. Kim, H.-H. Yang, C. Jung, H.G. Park, J.-B. Yoon, Y.-K. Choi, An electrostatic micromechanical biosensor for electrical detection of label-free DNA, Appl. Phys. Lett. 100 (2012) 163701.
[40] C.T. Lin, P.T.K. Loan, T.Y. Chen, K.K. Liu, C.H. Chen, K.H. Wei, L.J. Li, Label-free electrical detection of DNA hybridization on graphene using hall effect measurements: revisiting the sensing mechanism, Adv. Funct. Mater. 23 (2013) 2301–2307.
[41] Y. Mandabi, D. Fink, L. Alfonta, Label-free DNA detection using the narrow side of funnel-type etched nanopores, Biosens. Bioelectron. 42 (2013) 362–366.
[42] S. Sorgenfrei, C.-y. Chiu, R.L. Gonzalez Jr., Y.-J. Yu, P. Kim, C. Nuckolls, K.L. Shepard, Label-free single-molecule detection of DNA-hybridization kinetics with a carbon nanotube field-effect transistor, Nat. Nanotechnol. 6 (2011) 126–132.
[43] G. Wenga, E. Jacques, A.C. Salaun, R. Rogel, L. Pichon, F. Geneste, Step-gate polysilicon nanowires field effect transistor compatible with CMOS technology for label-free DNA biosensor, Biosens. Bioelectron. 40 (2013) 141–146.
[44] X. Chen, C.Y. Hong, Y.H. Lin, J.H. Chen, G.N. Chen, H.H. Yang, Enzyme-free and label-free ultrasensitive electrochemical detection of human immunodeficiency virus DNA in biological samples based on long-range self-assembled DNA nanostructures, Anal. Chem. 84 (2012) 8277–8283.
[45] E. Dubuisson, Z. Yang, K.P. Loh, Optimizing label-free DNA electrical detection on graphene platform, Anal. Chem. 83 (2011) 2452–2460.
[46] R.M. Kong, Z.L. Song, H.M. Meng, X.B. Zhang, G.L. Shen, R.Q. Yu, A label-free electrochemical biosensor for highly sensitive and selective detection of DNA via a dual-amplified strategy, Biosens. Bioelectron. 54 (2014) 442–447.
[47] P. Lin, X.T. Luo, I.M. Hsing, F. Yan, Organic Electrochemical Transistors Integrated in Flexible Microfluidic Systems and Used for Label-Free DNA Sensing, Adv. Mater. 23 (2011) 4035-+.
[48] N.Y. Wu, W. Gao, X.L. He, Z. Chang, M.T. Xu, Direct electrochemical sensor for label-free DNA detection based on zero current potentiometry, Biosens. Bioelectron. 39 (2013) 210–214.
[49] S. Bi, L. Li, Y.Y. Cui, Exonuclease-assisted cascaded recycling amplification for label-free detection of DNA, Chem. Commun. 48 (2012) 1018–1020.
[50] F.L. Gao, J.P. Lei, H.X. Ju, Label-free surface-enhanced Raman spectroscopy for sensitive DNA detection by DNA-mediated silver nanoparticle growth, Anal. Chem. 85 (2013) 11788–11793.
[51] H. Im, H.L. Shao, Y.I. Park, V.M. Peterson, C.M. Castro, R. Weissleder, H. Lee, Label-free detection and molecular profiling of exosomes with a nano-plasmonic sensor, Nat. Biotechnol. 32 (2014) (490-U219).
[52] W.Z. Shen, M.Z. Li, B.L. Wang, J. Liu, Z.Y. Li, L. Jiang, Y.L. Song, Hierarchical optical antenna: gold nanoparticle-modified photonic crystal for highly-sensitive label-free DNA detection, J. Mater. Chem. 22 (2012) 8127–8133.
[53] Y. Tao, Y.H. Lin, Z.Z. Huang, J.S. Ren, X.G. Qu, DNA-templated silver nanoclusters-graphene oxide nanohybrid materials: a platform for label-free and sensitive fluorescence turn-on detection of multiple nucleic acid targets, Analyst 137 (2012) 2588–2592.
[54] C.Q. Zhao, L. Wu, J.S. Ren, X.G. Qu, A label-free fluorescent turn-on enzymatic amplification assay for DNA detection using ligand-responsive G-quadruplex formation, Chem. Commun. 47 (2011) 5461–5463.
[55] D.C. Marcano, D.V. Kosynkin, J.M. Berlin, A. Sinitskii, Z.Z. Sun, A. Slesarev, L.B. Alemany, W. Lu, J.M. Tour, Improved synthesis of graphene oxide, ACS Nano 4 (2010) 4806–4814.
[56] X.Y. Chen, H.C. Guo, T. Wang, M. Lu, T.H. Wang, In-situ fabrication of reduced graphene oxide (rGO)/ZnO heterostructure: surface functional groups induced electrical properties, Electrochim. Acta 196 (2016) 558–564.
[57] F. Tuinstra, J.L. Koenig, Raman spectrum of graphite, J. Chem. Phys. 53 (1970) 1126–1130.
[58] A.C. Ferrari, J.C. Meyer, V. Scardaci, C. Casiraghi, M. Lazzeri, F. Mauri, S. Piscanec, D. Jiang, K.S. Novoselov, S. Roth, A.K. Geim, Raman spectrum of graphene and graphene layers, Phys. Rev. Lett. 97 (2006) 187401.
[59] A. Gupta, G. Chen, P. Joshi, S. Tadigadapa, P.C. Eklund, Raman scattering from high-frequency phonons in supported n-graphene layer films, Nano Lett. 6 (2006) 2667–2673.
[60] D.C. Marcano, D.V. Kosynkin, J.M. Berlin, A. Sinitskii, Z.Z. Sun, A. Slesarev, L.B. Alemany, W. Lu, J.M. Tour, Improved synthesis of graphene oxide, ACS Nano 4 (2010) 4806–4814.
[61] J.P. Zhao, S.F. Pei, W.C. Ren, L.B. Gao, H.M. Cheng, Efficient preparation of large-area graphene oxide sheets for transparent conductive films, ACS Nano 4 (2010) 5245–5252.
[62] H.A. Becerril, J. Mao, Z. Liu, R.M. Stoltenberg, Z. Bao, Y. Chen, Evaluation of solution-processed reduced graphene oxide films as transparent conductors, ACS Nano 2 (2008) 463–470.
[63] X. Wang, L.J. Zhi, K. Mullen, Transparent, conductive graphene electrodes for dye-sensitized solar cells, Nano Lett. 8 (2008) 323–327.
[64] H.T. Liu, L. Zhang, Y.L. Guo, C. Cheng, L.J. Yang, L. Jiang, G. Yu, W.P. Hu, Y.Q. Liu, D.B. Zhu, Reduction of graphene oxide to highly conductive graphene by Lawesson's reagent and its electrical applications, J. Mater. Chem. C 1 (2013) 3104–3109.
[65] B. Nandy, M. Santosh, P.K. Maiti, Interaction of nucleic acids with carbon nanotubes and dendrimers, J. Biosci. 37 (2012) 457–474.
[66] M. Zheng, A. Jagota, M.S. Strano, A.P. Santos, P. Barone, S.G. Chou, B.A. Diner, M.S. Dresselhaus, R.S. Mclean, G.B. Onoa, Structure-based carbon nanotube sorting by sequence-dependent DNA assembly, Science 302 (2003) 1545–1548.
[67] C.H. Lu, H.H. Yang, C.L. Zhu, X. Chen, G.N. Chen, A graphene platform for sensing biomolecules, Angew. Chem. Int. Ed. 48 (2009) 4785–4787.